1

Introduction and Literature Review

This chapter starts with enabling keys of channel capacity and their limitations in the communication channel links and further investigates the MIMO system's utility in the same channel model. The responsible factors which ensure large channel capacity and high spectral efficiency are also discussed. This thesis also explores the overview and analytical formulation of the monopole antenna, which is one of the suitable structures for portable user's devices. Further, it introduces an extensive investigation on MIMO antenna and its performance metrics, which will ensure the correct behaviour. Furthermore, various sources of electromagnetic coupling and diversity techniques are detailed in this chapter. Later, an extensive literature review is carried out on the 2-element, 4-element, and 8-element MIMO antennas, and their pros and cons were also identified. The utility of some known coupling reduction techniques between antenna elements has also been discussed. Finally, corresponding to these identified findings, some high-order MIMO structures at different frequency operations are investigated to explore the research gap, which is the objective of this thesis.

1.1 Introduction

The last few decades have seen astounding development in wireless communication technology, resulting in fulfilling the requirement of continuously increasing the demand for a high data rate in people's life. Simultaneously, the need for low-profile/compact communication devices increases after growing from 1G (One-Generation) to 5G (Fifth-Generation) word wide. The 'antennas' are the mainstay for the wireless system; as per IEEE Standard definitions [IEEE std (145-1983)], an antenna is defined as "a means for radiating and receiving radio waves" [1]. Therefore, the immense of wireless devices require compact, low-profile antennas without compromising their performance, which is a key element for channel capacity in the communication channel model. The channel capacity is calculated using Shannon's channel capacity theorem [2].

$$C = BW \log_2(1 + SNR) \text{ bits/s/Hz} \tag{1.1}$$

where, C = channel capacity (bits/s),

BW = bandwidth (Hz), and

SNR = the signal to noise ratio.

In the wireless communication system, channel capacity increases either by increasing the operating bandwidth or by increasing the system's signal-to-noise ratio. The bandwidth can be enhanced by increasing the modulated carrier's symbol rate, which is more liable for multipath fading. The signal-to-noise ratio can be increased under a specified limit because the wireless system introduces the noise in the channel. In contrast, an increase in bandwidth also increases the transmission power. As a result, the single antenna systems have multipath fading, low capacity, and low bandwidth. These are the trade-off in Shannon's channel capacity theorem for the single antenna system.

1.2 Motivation

The technological growth in the areas of modern wireless communication, investigation mainly focuses on obtaining a higher and higher data rate without compromising any other aspect, which is further possible by increasing the number of antenna elements in the transmitter and receiver of the wireless communication system in place of the single antenna system on the same channel model. As a result, Multiple Input Multiple Output (MIMO) antenna systems are demanding instead of Single Input Single Output (SISO), Single Input Multiple Output (SIMO), and Multiple Input Single Output (MISO) antennas in the communication system. That is one of the keys enabling technologies to increase the channel capacity with throughput, enhance data rate, and provide reliable communication. The channel capacity may be linearly improved by increasing the antenna elements in the MIMO system without gaining additional bandwidth and power consumption and allowing the transmission of independent data streams from multiple antennas on the same frequencies without misinterpreting the data signals. This aspect makes the researchers/scientists/engineers more curious about MIMO antenna research, thinking about further advancement of MIMO antennas and its performances. This scope has motivated the author to design, develop, fabricate, and measure some compact, low-profile high-order MIMO antennas for the present thesis work.

1.3 MIMO System

The history of MIMO technology begins with the publication of Winters in 1984 [3]. Later, some research papers and patents were published by some researchers (Paulraj and Kailath in 1994, Foshchini in 1996, Raleigh and Cioffi in 1998, Raleigh and Jones in 1999, and Golden *et al.* in 1999) to understand the advancement in the MIMO system [4]–[8]. Multiple antenna elements are utilized in the MIMO system at both ends of the

wireless system link, i.e., M numbers of transmit antennas (T_X) and N numbers of receive antennas (R_X). Therefore, an (M×N) number of independent data streams became between the transmitter and receiver channel module by utilizing spatial multiplexing at the same operating frequency. As a result, wireless link's channel capacity and spectral efficiency improved without additional bandwidth and transmitted power consumption.

1.3.1 Channel Capacity of MIMO Links

Fig. 1.1 shows the multiple antenna links model of the (M×N) MIMO antenna system. Let us assume that the channel includes multipath fading (including scattering) between the transmitter and receiver channel link. The presented channel link is modelled by a mathematical Eq. (1.2).

$$Y = HX + n \tag{1.2}$$

where, Y = output signal vector,

X = input signal vector,

$H = h_{rt}$ channel matrics between transmitter and receiver antennas, and

n = additive white Gaussian noise (AWGN) vector.

The elements of channel matrix H are presented in Eq. (1.3) [9].

$$H = \begin{bmatrix} h_{11} & \cdots & h_{1M} \\ \vdots & \ddots & \vdots \\ h_{N1} & \cdots & h_{NM} \end{bmatrix} \tag{1.3}$$

Each H element can be decomposed into two components, as shown in Eq. (1.4).

$$h_{rt} = S_{ij} = S_{ij}^{d} + S_{ij}^{m} \tag{1.4}$$

where, $h_{rt} \in r = 1, ..., N$; $t = 1, ..., M$ and

$S_{ij} \in j = 1, ..., M$; $i = M + 1, ..., M + N$ is the complex transmission coefficient between the j^{th} transmitting antenna and the i^{th} receiving antenna.

S_{ij}^{d} = direct component and S_{ij}^{m} = all multipath components.

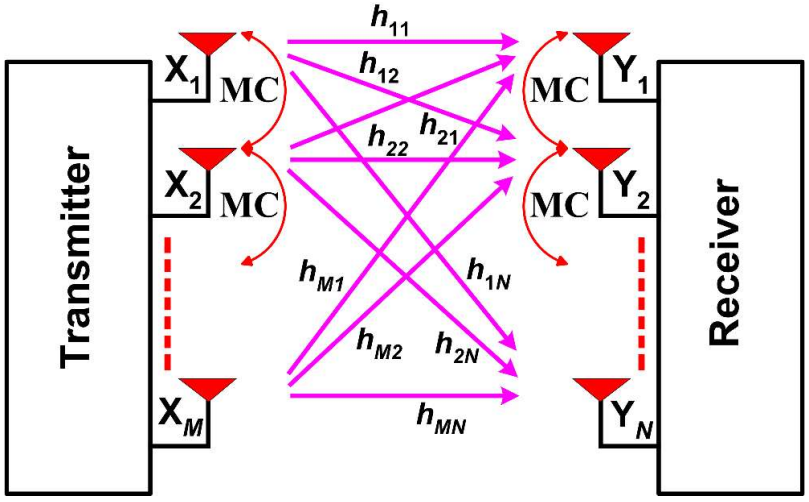

Fig. 1.1: MIMO system module with mutual coupling between antenna elements.

1.3.1.1 Channel State Information (CSI) at Transmitter

The channel capacity depends on allocating power to each subchannel. Theoretically, the CSI is assumed that it is known at the receiver of the channel link. However, the same consideration does not apply to the transmitter.

When the CSI is unknown at the transmitter end, the transmitted signal components are independent and equally allocated to each transmitting antenna. Hence, the power assigned to each of M the subchannel antennas is $p_k = p_t/M$. The capacity of (M×N) MIMO channel link without CSI is expressed in Eq. (1.5) and (1.6) [10], [11].

$$C = \log_2 \left\{ \left| \boldsymbol{I}_N + \frac{SNR}{M} \boldsymbol{H}\boldsymbol{H}^{\dagger} \right| \right\} \text{ bits/s/Hz} \tag{1.5}$$

$$C = \sum_{k=1}^{n} \log_2 \left\{ 1 + \frac{p_t}{M\sigma^2} \varepsilon_k^2 \right\} \text{ bits/s/Hz} \tag{1.6}$$

where, $\boldsymbol{I}$ = identity matrix,

† = conjugate transpose of a matrix, and

SNR = p_t/σ^2, where, p_t = total transmitted power allocated at transmitter link and

σ^2 = noise power.

The capacity estimation of a MIMO channel link is possible by using linear transformations at both the transmitter and receiver end, converting the MIMO channel to

$n = \min\{M, N\}$ SISO subchannels. $\varepsilon_k^2, k = 1, 2, \ldots\ldots, n$ are power gain allocated to the k^{th} subchannels, which are non-negative eigen values of the $\boldsymbol{HH}^{\dagger}$matrix.

When CSI is known at the transmitter of the channel link, it can perform to allocate optimum power allocation to the n subchannels in the channel links. The capacity of (M×N) MIMO channel link given in Eq. (1.6) is modified when the CSI is known is expressed in Eq. (1.7).

$$C = \sum_{k=1}^{n} \log_2 \left\{1 + \frac{\gamma_k p_t}{M\sigma^2} \varepsilon_k^2\right\} \quad \text{bits/s/Hz} \tag{1.7}$$

where, coefficient γ_k corresponds to the amount of power allocated to the k^{th} subchannel. This coefficient is given by Eq. (1.8) and also satisfies Eq. (1.9) for optimum γ_k.

$$\gamma_k = E\{|S_k|^2\} \tag{1.8}$$

$$\sum_{k=1}^{n} \gamma_k = M \tag{1.9}$$

The conclusion is that **i**) there are $M = N$ number of antennas at both ends of the channel link, the average capacity increases linearly with M antennas, and **ii**) otherwise will increase proportionally with the smallest number of antennas $\min\{M, N\} = n$ outside and on longer inside the log function. The average capacity is given in Eq. (1.10) [12].

$$C_a \approx M \log_2(1 + SNR) \text{ bits/s/Hz} \tag{1.10}$$

1.3.2 Spectral Efficiency

The spectral efficiency denotes SE measured in bits/sec/Hz, which measures how well the channel spectrum is used, is one of the essential criteria utilized to define wireless communication performance. The SE is defined for $k \rightarrow k'$ links in Eq. (1.11).

$$SE = \sum_{k=1}^{2K} \log_2(1 + SINR_k) \text{ bits/s/Hz} \tag{1.11}$$

where, there are $2K$ number of users in a network, p_k is transmitting power of k^{th} users and SINR_k denotes the signal-to-interference-noise ratio experienced by the k^{th} users.

Finally, it has been proven in Section 1.3.1 and 1.3.2 that the channel capacity and spectral efficiency of the MIMO system increases with the increase of number of antennas in the transmitter and receiver of the wireless communication system. Simultaneously, a new challenge of mutual coupling arises when embedding many antennas on size-restrained devices. As a result, coupling between antennas damages the orthogonality between the signal streams and thus reduces channel capacity. Besides, the impact of mutual coupling also deteriorates the antenna's impedance matching characteristics, radiation efficiency, and radiation pattern [13].

1.3.3 Mutual Coupling at Channel End

In the MIMO antennas or arrays, the electromagnetic interaction between antenna elements is defined as mutual coupling, denoted as *MC* measured by dB value of *S*-parameters between the i^{th} and j^{th} element $[(10\log_{10}|S_{ij}|)]$. It depends on the configuration of MIMO/array and excitations of elements. In this process, the electromagnetic wave is absorbed by one antenna when another antenna radiates an electromagnetic wave. As a result, coupling between them tends to change the behavior of impedance matching, reflection coefficient, radiation patterns, and radiation efficiency of the antenna elements. The empirical model to facilitate the mutual coupling C_{ij} is presented in Eq. (1.12) and (1.13) [13].

$$MC_{ij} = exp\left(-\frac{2d_{ij}}{\lambda}(\alpha + n\pi)\right), \qquad i \neq j \tag{1.12}$$

$$MC_{ij} = 1 - \frac{1}{N}\sum_i \sum_{i \neq j} MC_{ij} \tag{1.13}$$

where, d_{ij} = distance between i^{th} and j^{th} antenna elements, α = coupling level controlling parameter, and N = total number of the antenna element in the configuration.

The mechanisms of mutual coupling in the transmitting and receiving modes are discussed in the following section [14].

1.3.3.1 Mutual Coupling in the Transmitting Mode

Fig. 1.2(a) shows different energy pathways in transmitting mode, where electromagnetic waves interact indirectly through scattering parameters (like transmission coefficients S_{ji}) between closely spaced i^{th} and j^{th} antennas. Let's assume an active source is connected with the j^{th} antenna element in an array configuration. The amount of energy released by the source (1↑) radiates in free space (2↑) and toward i^{th} antenna element (3←). Part of the energy received by the i^{th} antenna element is rescattered in the free space (4↑), and the remaining amount of energy travels toward the i^{th} antenna source (5↓). A few amounts of rescattered energy (6→) will be travelled toward the j^{th} antenna element.

The conclusion is that **i**) this interaction process will continue indefinitely. After a few iterations, rescattered energy (4↑) decreases significantly. The total far-field is the vector sum of rescattered and radiated fields. Hence, mutual coupling tends to change the radiation pattern of the antenna, **ii**) the wave (5↓) is vectorially added to reflected and incident waves of i^{th} element itself; as a result, improvement in the standing wave that is accountable for changing the input impedance of i^{th} antenna element. Hence mutual coupling changes the antenna's self-impedance and mutual impedance, and **iii**) in the MIMO system, each antenna element may have individual and random phase excitation. Due to this, the impedance matching and mutual coupling are affected significantly, which is analysed by the total active reflection coefficient (TARC). The TARC measures the effectiveness of the reflection coefficient with random phase excitation of the antenna elements. It is the ratio of the square root of the total generated power by all port excitations minus the total radiated power and the total generated power [15]. Higher mutual coupling is responsible for poor TARC. As a result, it reduces the radiation efficiency due to its accountability on mutual coupling and impedance matching under random phase excitation of different ports.

1.3.3.2 Mutual Coupling in the Receiving Mode

Fig. 1.2(b) shows different energy pathways in receiving mode. It is assumed that a plane wave (1↘) impinges onto the antenna array configuration, first arriving at i^{th} antenna element, causing induces a current. A part of the current travels toward the receiver (2↓), and the rest is rescattered in free space (3↑). A few parts of the rescattered wave travel toward the j^{th} antenna element (4→), which is vertically added with plane incident wave (5↑). As a result, the wave received by i^{th} antenna element is the vector sum of the direct incident wave, and coupled waves come from the j^{th} antenna element. The received energy can be maximized by minimizing the rescattered wave energy. However, the terminating impedance of i^{th} antenna element must be selected carefully as the reflected wave (5↑) is cancelled out by the rescattered wave (3↑). Further, the antenna element's performance can be investigated in receiving mode when an active source is connected to the i^{th} antenna element (excited) and other j^{th} antenna elements are kept a passive source (terminated with 50-ohm loads).

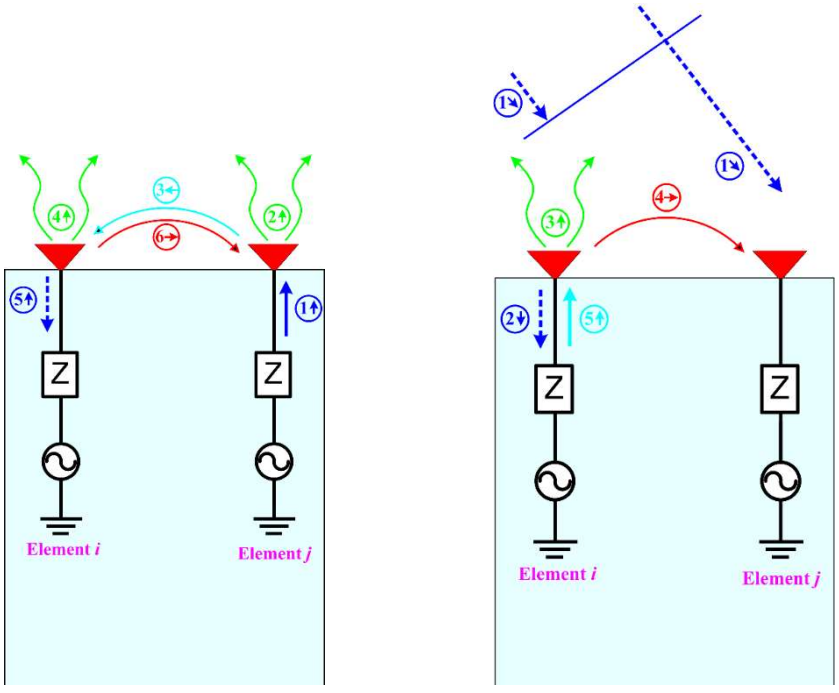

(a) (b)

Fig. 1.2: Mutual coupling between antenna elements (a) transmitting mode and (b) receiving mode.

1.4 Antenna Structures Used in Portable Devices

The demand for new technological features in modern wireless devices is increasing day by day. As a result, modern wireless communication systems are equipped with the latest technologies that make people's lives more pleasant. Over the past two decades (from 1G to 5G), as the number of wireless devices, i.e., smartphones, tablets, smartwatches, etc., have become more compact and low-profile. Hence, there is a need for compact/low-profile/multiple antennas increases. Today's modern wireless devices must not only meet the challenging technical needs of internet of things (IoT) applications. Still, they must also have high-quality speakers, large HD (high-definition) display, long battery life, and be aesthetically pleasing. Also, they should fit comfortably in one's hand while still being slim enough to make handy. These needs present unique challenges to researchers/engineers. The primary challenge associated with the design of antennas for compact/low-profile wireless communication devices is limited available space, multiband frequency operations, the ability to embed with other components of the devices, and packaging.

Advancements and development in manufacturing technology have empowered electrical components to reduce in size rapidly over the past several decades. Although electronic component sizes in the equipment have been steadily decreasing following Moore's Law, antenna size that supports these devices may not follow the same trend. The antennas are defined fundamentally not by manufacturing technology but by the underlying physics governing their operation.

According to the wave propagation principle, the radiative potential of an antenna depends on its wavelength for the desired operating frequency. Antennas involved in wireless portable devices like smartphones are often considered to be electrically small because they are configured to fit into volumes much lesser than their operational

wavelength. However, electrically small antennas (ESA's) are utilized in mobile communication applications and are much smaller than their operating frequency. Still, they face few fundamental trade-offs as the size of the antenna is always inversely associated with its impedance bandwidth, gain, and efficiency. A small antenna can be optimized for a fractional wavelength size, and then the antenna will suffer from poor efficiency and narrow bandwidth. These fundamental trade-offs give rise to many diverse and unique solutions for antennas involved in wireless communications technology. Therefore, more unusual techniques must be investigated to reduce size without affecting other performances. Some of the essential factors needed in antenna design for modern communication devices are as follows.

- Small size and low-profile
- Robustness and flexibility
- Multiband operation
- Integration with nearby components
- Multi-element capability
- Capability of packaging

Ultimately one of the foremost goals of the antenna engineers is to configure a printed planar, compact, low-profile, and multifunctional antenna that can easily be integrated with compact portable devices and is suitable for MIMO configuration. As per the literature, some antennas are generally utilized in wireless portable devices, the planar inverted-F antenna, dipole antenna, and monopole antenna; in some cases, hybrid designs use more than one of the prime geometric structures. Specifically, the monopole antenna is integrated inside the portable devices, as shown in Fig. 1.3. The thesis is primarily devoted to analyses and modelling the printed planar monopole antenna utilized to configure the MIMO antenna, which is realized with portable devices.

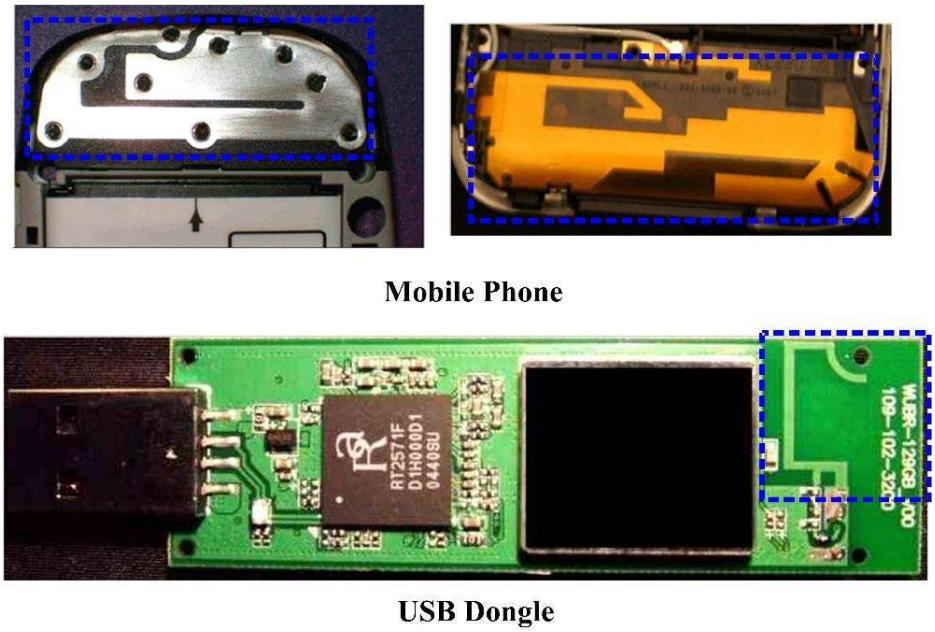

Fig. 1.3: Printed monopole antenna inside portable devices.

1.5 Monopole Antenna

Guglielmo Marconi invented the monopole antenna in the year of 1895. A straight wire-shaped conductor was installed perpendicularly at the top of the perfectly conductive surface. A monopole antenna is a modified form of dipole antenna where transmission or radiation of the electromagnetic energy takes place using two terminals. The half-wave dipole has symmetrical terminals of length equal to λ/2 at the corresponding operating frequency. Monopole antenna has a single radiating terminal of length equal to λ/4 (half-length of the dipole) on the ground plane and creates a virtual symmetrical terminal below the ground plane. The half-wave dipole and its corresponding monopole antenna are illustrated in Fig. 1.4.

1.5.1 Principle of Monopole Antenna

The monopole antenna configuration is derived from the dipole antenna by utilizing the image theory. According to the image theory, a vertical arm of the dipole (quarter-wavelength) is placed perpendicular to the sizeable conducting ground plane, and reflections from the ground plane produce a "virtual quarter-wavelength" below the

ground, as considered dipole is shown in Fig. 1.5. As a result, a monopole antenna's input impedance and radiation resistance are half the value of the corresponding dipole, and directivity is just twice due to the radiation in the upper half only [16]. That has vertical polarization and horizontal omnidirectional radiation patterns. The flowing current on the monopole is the same as on the upper arm of its dipole counterpart, but the terminal voltage is only half of the corresponding dipole. The gap width of the input terminal is half of the considered dipole, and the same electric field over the upper half-length provides a half voltage and half power radiated the corresponding that. Therefore, the monopole's input impedance and radiation resistance are half of the corresponding dipole, as given in Eq. (1.14) and (1.15).

1.5.2 Printed Planar Monopole Antenna

The impedance bandwidth of such wire dipole and monopole antennas can be enhanced by increasing the radius of the wire or, in other words, the volume it occupies [17]. With this standard rule, wire dipole and monopole antennas are modified to get wider bandwidth in myriad ways. Some of these modified typical non-planar antenna structures were cage, conical, and helical monopole, which provided enhanced bandwidth. Still, they were bulkier, not compatible with portable devices, and more expensive. Therefore, these non-planar antenna structures have been replaced by the planar monopole antennas designed through PCB (printed circuit board) technology to broaden impedance bandwidth. These are widely used in wireless communication devices because of their inherent advantages: low-profile, planar structure, low-cost fabrication, and easy integration with other circuit components. A non-planar monopole antenna modifies the planar wire monopole to broader the impedance bandwidth. Further, the planar monopole is modified by a printed planar monopole antenna by utilizing PCB technology, as shown in Fig. 1.6.

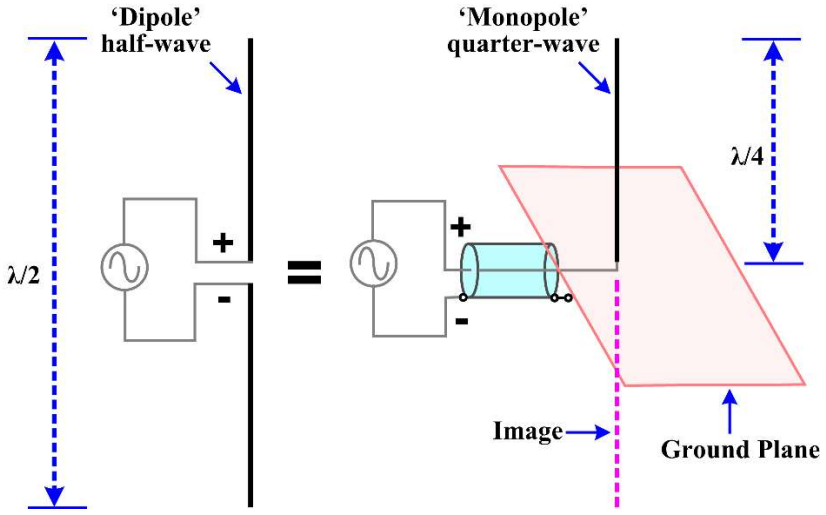

(a) (b)

Fig. 1.4: Basic structure of (a) dipole and (b) monopole antenna.

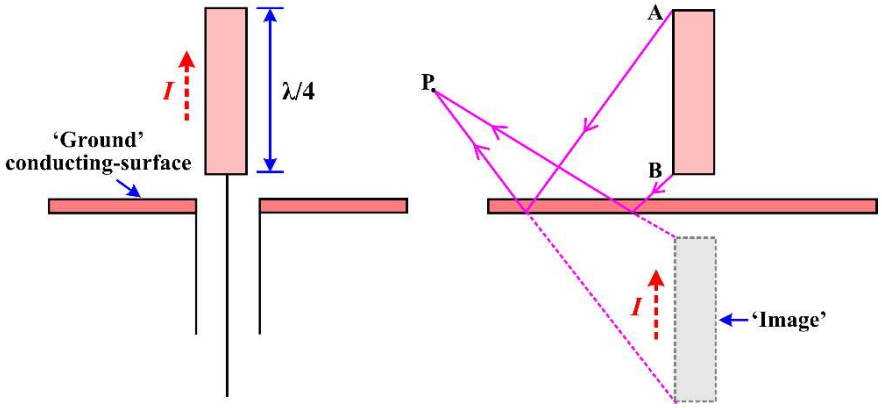

(a) (b)

Fig. 1.5: Basic configuration (a) monopole and (b) equivalent dipole.

$$Z_{in} = \frac{V_{in,mono}}{I_{in,mono}} = \frac{\frac{1}{2}V_{in,dipole}}{I_{in,dipole}} = \frac{1}{2}Z_{in,dipole} \tag{1.14}$$

$$R_{r,mono} = \frac{P_{rad,mono}}{\frac{1}{2}|I_{in,mono}|^2} = \frac{\frac{1}{2}P_{rad,dipole}}{\frac{1}{2}|I_{in,dipole}|^2} = \frac{1}{2}R_{r,dipole} \tag{1.15}$$

The wideband impedance bandwidth is obtained in the printed planar monopole antenna structures (PPMA) mainly due to two factors. One is reducing the quality factor 'Q' possible due to the broad radiating patches by replacing thin wire and using low losses substrate. Second, a finite ground plane can support higher resonating modes and the fundamental quarter wavelength mode. The overlapping of the various modes with significant impedance matching is responsible for the wideband impedance bandwidth, as

illustrated in Fig. 1.7. The fundamental mode exists when the operating wavelength is larger than the antenna size (applicable for lowest resonant frequency), and the high-order modes exist when the operating wavelength becomes smaller than antenna size (useful for higher frequencies) [18].

1.5.3 Mathematical Formulation for Resonant Frequency

The mathematical formula to obtain the fundamental resonant frequency of any planar monopole antenna can be calculated by the transformation of the wire monopole. For example, the fundamental resonant frequency of the planar rectangular monopole is calculated by modifying thin cylindrical wire monopole [Kumar and Ray (1981)] [19].

By equating the area of the rectangular planar structure to that of an equivalent thin cylindrical of the same radius '*r*' and length '*L*', as shown in Fig. 1.8.

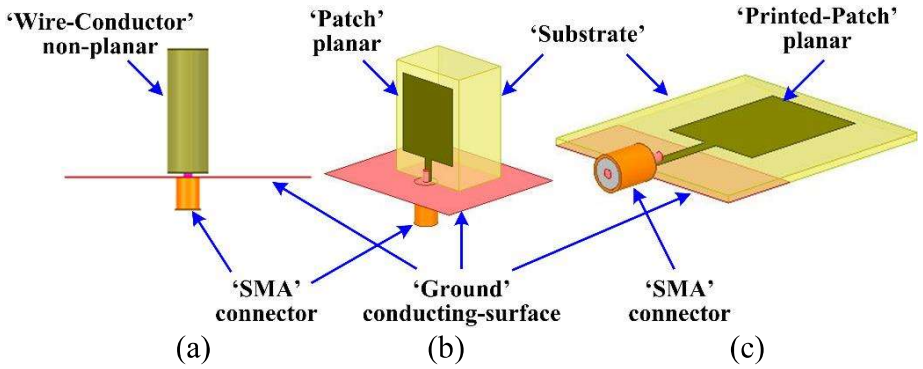

Fig. 1.6: Types of monopole structures (a) wire-monopole, (b) planar-monopole, and (c) printed planar-monopole.

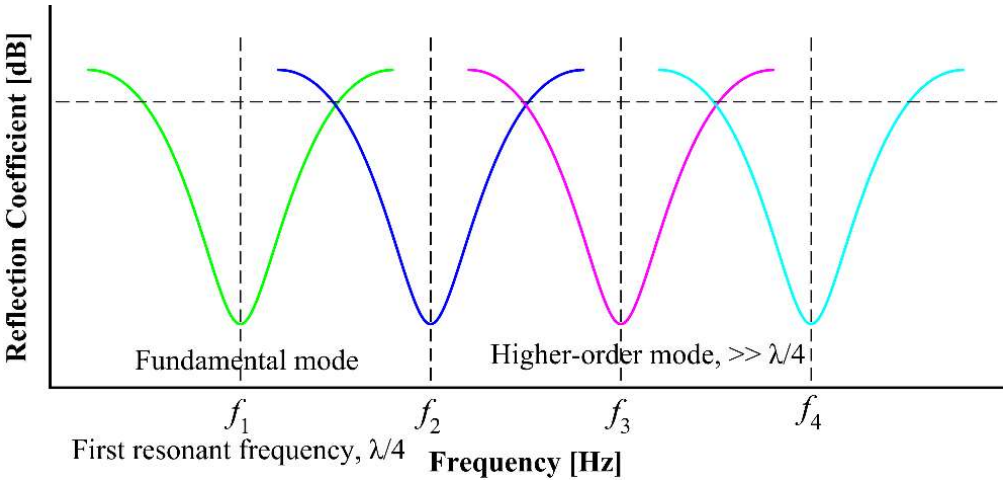

Fig. 1.7: Overlapping modes in printed planar monopole structure.

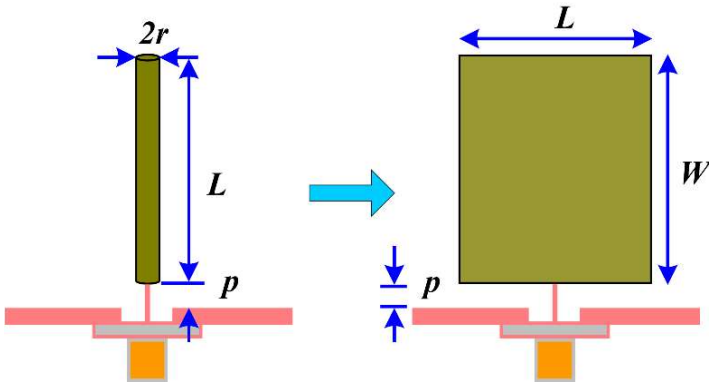

Fig. 1.8: Thin cylindrical wire monopole to rectangular planar monopole structure.

$$2\pi rL = LW \tag{1.16}$$

where, L is the length and W is the width of the rectangular planar patch. Eq. (1.16) gives,

$$r = W/2\pi \tag{1.17}$$

Eq. (1.14) proves that the input impedance of the monopole antenna 'λ/4' is half that of the dipole antenna 'λ/2'. Thus, the value of input impedance is 36.5 + j 21.25 Ω for an infinitesimally thin monopole antenna that is inductive. The real value of input impedance is obtained when a slightly smaller length of the monopole is used, as given in [1].

$$L = 0.24\lambda F' \tag{1.18}$$

where, $F' = (L/r)/(1 + L/r) = L/(L+ r)$

Putting in Eq. (1.18), the wavelength 'λ' is obtained as,

$$\lambda = (L + r)/0.24 \tag{1.19}$$

Thus, the first resonant frequency (f_r) is calculated using Eq. (1.20).

$$f_r = c / \lambda = 30 / \lambda = 7.2 / (L + r)\ \text{GHz} \tag{1.20}$$

where, r, L, and λ are in centimetres.

Eq. (1.20) does not consider the length of probe 'p' the influence of the probe length responsible for reducing the frequency toward lower due to, the Eq. (1.20) is modified as,

$$f_r = 7.2 / (L + r + p)\ \text{GHz} \tag{1.21}$$

where, p is the probe length (the gap between the rectangular monopole and ground plane) in centimetre.

The radiation pattern of a monopole antenna is more like a dipole pattern, so a planar printed monopole antenna can be equivalent as a printed dipole of length, including the length of the ground plane. All printed monopoles are under dipole effect with a fundamental resonant frequency, and the height of the ground plane contributes to determining the resonant frequency. The dielectric constant of the substrate at which antennas are printed also contributes to deciding the resonant frequency.

Hence, the fundamental resonant frequency of the planar printed rectangular monopole is approximated by considering the cylindrical wire monopole [20].

By equating the area of the rectangular printed planar structure to that of cylindrical wire of length 'h' and radius 'r', as shown in Fig. 1.9.

$$2\pi rh = lw = area \tag{1.22}$$

Since, $h = l\sqrt{\varepsilon_{reff}}$

Equating in Eq. (1.22) gives

$$r = area/2\pi l\sqrt{\varepsilon_{reff}} \tag{1.23}$$

where l is the length and w is the width of the rectangular printed planar patch. ε_{reff} is substrate effective relative dielectric constant. The length of the cylindrical dipole for real input impedance at first resonance is given in [1].

$$l = 0.48\lambda F \tag{1.24}$$

where, $F = (l/2r)/(1 + l/2r) = l/(l + 2r)$ from Eq. (1.18).

Equating in Eq. (1.24) gives wavelength λ, that is

$$\lambda = (l + 2r)/0.48 \tag{1.25}$$

Therefore, the first resonant frequency f_r is calculated by Eq. (1.20).

$$f_r = 14.4 / (L + 2r) \text{ GHz} \tag{1.26}$$

where, l and r are in centimetres.

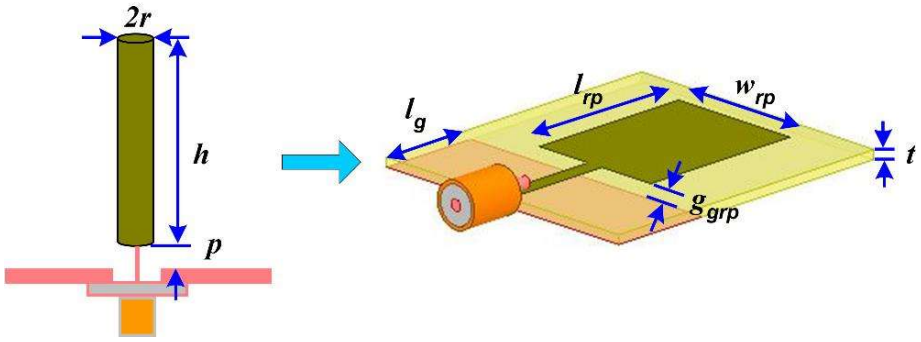

Fig. 1.9: Cylindrical wire monopole to rectangular printed planar monopole structure.

If l_g and l_{rp} are ground and radiating patch length in centimetre, respectively. g_{grp} is gap length between ground and radiating patch in centimetre. Then l can be denoted as $l_g + l_{rp} + g_{grp}$. Similarly, if r_1 and r_2 are represent the radius of equivalent cylindrical dipole corresponding to the ground plane and radiating patch, then $2r$ can be denoted as r_1 and r_2 (r_1 and r_1 can be considered as the radius of dipole arms and can be expressed as $r_1 = r_2 = r$).

From Eq. (1.23),

$$r_1 = A_g / 2\pi l_g \sqrt{\varepsilon_{reff}} \tag{1.27}$$

$$r_2 = A_{rp} / 2\pi l_{rp} \sqrt{\varepsilon_{reff}} \tag{1.28}$$

where, A_g and A_{rp} are ground and radiating patch acquired areas in centimeters^2.

Hence, the fundamental resonant frequency,

$$f_r = \frac{14.4}{l_g + l_{rp} + g_{grp} + \frac{A_g}{2\pi l_g \sqrt{\varepsilon_{reff}}} + \frac{A_{rp}}{2\pi l_{rp} \sqrt{\varepsilon_{reff}}}} \text{ GHz} \tag{1.29}$$

1.6 MIMO Antenna Implementing Challenges

The use of multiple antennas on both the transmitter and receiver sides has gained interest over the past decade. The number of antenna elements needs to be increased at the base station side as well as at the user terminal. It can easily be accomplished on the base station side, but it is very challenging on the user side. The number of antenna elements is

expected to grow in handheld devices to increase the data rate and spectral efficiency, but it poses some challenges to the antenna designer.

- Integrate the highest number of antenna elements in the MIMO antenna configuration with size, space, profile, and performance constraints.
- Reduce port coupling between a pair of adjacent antenna elements needed for better efficiency.
- Minimize the field coupling to reduce the correlation among several MIMO channels.
- Improving diversity gain is utilized to enhance the quality and reliability of a wireless channel link.
- Good total active reflection coefficient values ensure adequate bandwidth robustness.

However, it is pretty challenging to configure a multi-standard low-profile MIMO antenna (multiple antenna elements) with the strict constraints of the physical size of user devices. Therefore, these challenges arise in the MIMO antenna design are characterized by analyzing the MIMO antenna's conventional and diversity performance parameter metrics, which is necessary for practical scenarios.

1.7 MIMO Antenna Performance Metrics

To realize the correct behavior of the MIMO antenna system, the study of several metrics (characteristics and diversity parameters) is a necessity for the practical scenario that has not been used in a conventional SISO antenna system. Along with the antenna's conventional performance parameters like resonance frequency, impedance bandwidth, radiation patterns, gain, and efficiency, several vital parameters must be analyzed to characterize the MIMO antenna. These metrics are not required in single-antenna devices, but these are necessary for multiple-antenna devices. These performance metrics are subdivided into two parts; characteristics and diversity, which are essential for the MIMO antenna.

1.7.1 Conventional Performance Metrics as Efficiency

The efficiency of the practical MIMO antenna is an important parameter relative to the ideal reference antenna having 100% efficiency. In MIMO antenna, efficiency increases by increasing the antenna elements. Suppose i^{th} element of the MIMO antenna consider as a reference antenna having 100% efficiency. What will be the actual efficiency of MIMO antenna with a combination of multiple antenna elements that can be elaborated in terms of radiation, mismatch, total, and multiplexing efficiency, which are needed for knowing the practical efficiency of the MIMO antenna?

1.7.1.1 Total Efficiency

In the *N*-elements MIMO antenna, the efficiency of a single i^{th} element is defined by radiation efficiency, which is same as any conventional antenna. The radiation efficiency is the ratio of total radiated power to total accepted power by i^{th} element of the MIMO system [21]. An essential term for efficiency is the power loss caused by mutual coupling between adjacent antenna elements [22]. The total efficiency of i^{th} element in the MIMO antenna is the multiplication of mismatch efficiency (due to mutual coupling between adjacent antenna elements) and radiation efficiency (which includes conduction and dielectric losses) [23].

$$\eta_{tot(i)} = \eta_{rad(i)}\eta_{mis(i)} \tag{1.30}$$

$$\eta_{mis(i)} = \left(1 - \sum_{j=1}^{N} \left|S_{ij}\right|^2\right) \tag{1.31}$$

where $\eta_{tot(i)}$, $\eta_{rad(i)}$, and $\eta_{mis(i)}$ is total, radiation, and mismatch efficiency of i^{th} antenna element respectively, N is the number of elements in the MIMO antenna, S_{ij} is *S*-parameter value from element i^{th} to element j^{th} ($1 \leq i \leq N$).

1.7.1.2 Multiplexing Efficiency

Similarly, in the *N*-elements MIMO antenna, the multiplexing efficiency is used to estimate the effectiveness of practical MIMO antenna with respect to ideal reference MIMO antenna having zero correlation and 100% total efficiency. The multiplexing efficiency is the ratio of necessitating signal-to-noise-ratio (SNR) between the practical MIMO antenna to the ideal reference MIMO antenna for resulting same capacity in the same independent and identically distributed (i.i.d.) channel relative to the reference antenna [24]. The multiplexing efficiency ($\tilde{\eta}_{mux}$) is estimated for high SNRs by using Eq. (1.31) [25], that is,

$$\tilde{\eta}_{mux} = \left(\prod_{i=1}^{N} \eta_{tot(i)}\right)^{\frac{1}{N}} \det(\overline{R})^{\frac{1}{N}} \tag{1.32}$$

where $\overline{R}$ is the normalized correlation matrix having diagonal elements value equal to one and $(i, j)^{\text{th}}$ $(i \neq j)$ elements of normalized correlation matrics are proposed in terms of the complex correlation coefficient $\rho_c(i, j, N)$ between i^{th} and j^{th} elements.

The normalized correlation matrix can be elaborated for the 8×8 MIMO antenna, that is,

$$\overline{R} = \begin{bmatrix} 1 & \rho_c(1,2,8) & \rho_c(1,3,8) & \rho_c(1,4,8) & \rho_c(1,5,8) & \rho_c(1,6,8) & \rho_c(1,7,8) & \rho_c(1,8,8) \\ \rho_c(2,1,8) & 1 & \rho_c(2,3,8) & \rho_c(2,4,8) & \rho_c(2,5,8) & \rho_c(2,6,8) & \rho_c(2,7,8) & \rho_c(2,8,8) \\ \rho_c(3,1,8) & \rho_c(3,2,8) & 1 & \rho_c(3,4,8) & \rho_c(3,5,8) & \rho_c(3,6,8) & \rho_c(3,7,8) & \rho_c(3,8,8) \\ \rho_c(4,1,8) & \rho_c(4,2,8) & \rho_c(4,3,8) & 1 & \rho_c(4,5,8) & \rho_c(4,6,8) & \rho_c(4,7,8) & \rho_c(4,8,8) \\ \rho_c(5,1,8) & \rho_c(5,2,8) & \rho_c(5,3,8) & \rho_c(5,4,8) & 1 & \rho_c(5,6,8) & \rho_c(5,7,8) & \rho_c(5,8,8) \\ \rho_c(6,1,8) & \rho_c(6,2,8) & \rho_c(6,3,8) & \rho_c(6,4,8) & \rho_c(6,5,8) & 1 & \rho_c(6,7,8) & \rho_c(6,8,8) \\ \rho_c(7,1,8) & \rho_c(7,2,8) & \rho_c(7,3,8) & \rho_c(7,4,8) & \rho_c(7,5,8) & \rho_c(7,6,8) & 1 & \rho_c(7,8,8) \\ \rho_c(8,1,8) & \rho_c(8,2,8) & \rho_c(8,3,8) & \rho_c(8,4,8) & \rho_c(8,5,8) & \rho_c(8,6,8) & \rho_c(8,7,8) & 1 \end{bmatrix}. \tag{1.33}$$

The complex correlation coefficients $\rho_c(i, j, N)$ is relatively correlated to the envelope correlation coefficient $\rho_e(i, j, N)$ for $(i, j)^{\text{th}}$ elements of MIMO antenna, such as complex correlation coefficients $\rho_c(i, j, N) = |\rho_e(i, j, N)|^{1/2}$ [24].

1.7.2 Non-Conventional Performance Metrics

The study of the non-conventional performance metrics is a necessity for a practical scenario, such as isolation (coupling), envelope correlation coefficient (ECC), diversity

gain (DG), mean effective gain (MEG), total active reflection coefficient (TARC), and channel capacity loss (CCL) to be evaluated in the following sections.

1.7.2.1 Isolation (Coupling)

In the literature, the terms isolation and coupling are usually interchanged as high isolation yields low coupling. It evaluates what amount of power is coupled from j^{th} element to i^{th} element when the port of i^{th} element is excited. More specifically, isolation is obtained directly from *S*-parameters ($-10log_{10}\left|S_{ij}\right|$) between i^{th} and j^{th} elements.

1.7.2.2 Envelope Correlation Coefficient (ECC)

The envelope correlation coefficient (ECC) evaluates the amount of correlation between antenna elements, ensuring the effectiveness of MIMO antenna performance, and a minimum value of ECC indicates greater pattern diversity. This metric also evaluates how much the radiation patterns are affected by one another when all antenna elements of the MIMO antenna operate simultaneously. The port-to-port mutual coupling effect between antenna elements of a MIMO antenna can be approximated using scattering parameters S_{in} and S_{nj}. The ECC can be calculated between the i^{th} and j^{th} element in the *N*-elements MIMO antenna by utilizing two methods: first using *S*-parameters [26] and second using 3-D complex field equations [27], that is,

$$ECC = \rho_e(i,j,N) = \frac{\left|\sum_{n=1}^{N} S_{i,n}^{*} S_{n,j}\right|^2}{\prod_{k=i,j}\left[1-\sum_{n=1}^{N} S_{k,n}^{*} S_{n,k}\right]} \tag{1.34}$$

$$ECC = \rho_e(i,j,N) = \frac{\left|\iint_{4\pi}[\overrightarrow{F_i}(\theta,\varphi)*\overrightarrow{F_j}(\theta,\varphi)]d\Omega\right|^2}{\iint_{4\pi}\left|\overrightarrow{F_i}(\theta,\varphi)\right|^2 d\Omega \iint_{4\pi}\left|\overrightarrow{F_j}(\theta,\varphi)\right|^2 d\Omega} \tag{1.35}$$

where $F_i(\theta,\varphi)$and $F_j(\theta,\varphi)$ are 3-D complex field patterns of i^{th} and j^{th} antenna element in the *N*-elements MIMO antenna, respectively. The value of ECC must be less than 0.5 for the practical MIMO system in the mitigating fading environment [23].

1.7.2.3 Diversity Gain (DG)

Diversity Gain (DG) is an important parameter for a MIMO antenna that must be taken into account while evaluating the MIMO performance. It measures the effect of diversity on the communication system and gives an idea about the reliability of the MIMO antenna. That is related to ECC. The lower value of the envelope correlation coefficient signifies a higher value of diversity gain. The DG between i^{th} and j^{th} element in *N*-elements MIMO antenna system is estimated by using the ECC parameters [14], that is,

$$DG = 10\sqrt{1 - |ECC|^2} = 10\sqrt{1 - |\rho_e(i,j,N)|^2} \tag{1.36}$$

1.7.2.4 Mean Effective Gain (MEG)

In wireless communications, the effective power of i^{th} element of the *N*-elements MIMO system in the rich fading environment can be estimated using the MEG. The MEG for i^{th} element of the MIMO antenna system is the ratio of mean received power ('P_{rec}') to mean incident power ('P_{inc}'). The MEG for i^{th} element in *N*-elements MIMO system is estimated by using propagation statistics and the radiation patterns [23].

$$MEG_i = \oint \left[\frac{XPR \cdot G_{\theta i}(\Omega) \cdot P_{\theta}(\Omega) + G_{\varphi i}(\Omega) \cdot P_{\varphi}(\Omega)}{1 + XPR} \right] d\Omega. \tag{1.37}$$

where Ω denote solid angle, *XPR* is cross-polarization power ratio, $G_{\theta i}(\Omega)$ and $G_{\varphi i}(\Omega)$ are the θ- and φ-polarized 3-D power gain patterns of the i^{th} element, $P_{\theta}(\Omega)$ and $P_{\varphi}(\Omega)$ are the θ- and φ-polarized components of angular power density, respectively. If the value of *XPR* = 1 and $P_{\theta}, P_{\varphi} = 1/4\pi$ are considered for a uniform propagation environment. Eq. (1.37) can be simplified [23], that is,

$$MEG_i = \frac{\eta_{tot(i)}}{2} \tag{1.38}$$

The ability of the *N*-element MIMO system in mitigating fading, the ratio of MEG_i/MEG_j must be close to unity and should not exceed ±3 dB [23].

1.7.2.5 Total Active Reflection Coefficient (TARC)

In a MIMO system, the scattering matrix is not sufficient to predict the behavior of the multi-element antenna. Thus, a generalized parameter total active reflection coefficient (TARC) is introduced for proper characterization of the multiport antenna system. In the *N*-element MIMO antenna, total active reflection coefficient (TARC) can be defined as the ratio of the square root of the incident power provided by all excited ports minus radiated power to the square root of the incident power [15]. The TARC of the *N*-elements MIMO antenna is estimated using the scattering matrix at all ports.

$$\Gamma_a^t = \sqrt{\sum_{i=1}^{N}|b_i|^2} / \sqrt{\sum_{i=1}^{N}|a_i|^2} \tag{1.39}$$

$$b = Sa \tag{1.40}$$

where a_i is the incident signal, b_i is the reflected signal, and S is the scattering matrix.

The TRAC value for N-elements MIMO antenna should satisfy following criteria, that is

$$0 < TARC < \Gamma_a^t < 1 \tag{1.41}$$

In contrast, the value of TARC zero means total power is radiated, and one means all power is either reflected back or goes to other ports, which means less than 1 or 0 dB value of TARC is required in the MIMO system [15].

Let's assume a case of 8 × 8 MIMO antenna, and scattering matrix can be elaborated as,

$$\begin{bmatrix} b_1 \\ b_2 \\ b_3 \\ b_4 \\ b_5 \\ b_6 \\ b_7 \\ b_8 \end{bmatrix} = \begin{bmatrix} S_{11} & S_{12} & S_{13} & S_{14} & S_{15} & S_{16} & S_{17} & S_{18} \\ S_{21} & S_{22} & S_{23} & S_{24} & S_{25} & S_{26} & S_{27} & S_{28} \\ S_{31} & S_{32} & S_{33} & S_{34} & S_{35} & S_{36} & S_{37} & S_{38} \\ S_{41} & S_{42} & S_{43} & S_{44} & S_{45} & S_{46} & S_{47} & S_{48} \\ S_{51} & S_{52} & S_{53} & S_{54} & S_{55} & S_{56} & S_{57} & S_{58} \\ S_{61} & S_{62} & S_{63} & S_{64} & S_{65} & S_{66} & S_{67} & S_{68} \\ S_{71} & S_{72} & S_{72} & S_{73} & S_{74} & S_{75} & S_{76} & S_{78} \\ S_{81} & S_{82} & S_{83} & S_{84} & S_{85} & S_{86} & S_{87} & S_{88} \end{bmatrix} \begin{bmatrix} a_1 \\ a_2 \\ a_3 \\ a_4 \\ a_5 \\ a_6 \\ a_7 \\ a_8 \end{bmatrix}. \tag{1.42}$$

Furthermore, to investigate the TARC of the MIMO antenna, the excitation of port-1 is kept at unity amplitude and zero phases ($1e^{j0}$), while the other elements (i.e., port-2, 3, 4, 5, 6, 7, and 8) are excited by similar amplitude and different phase excitations ($1e^{j\theta_i}$)

with i.i.d Gaussian random variable [28]. The TARC for 8×8 MIMO antenna is estimated from the scattering matrix using Eq. (1.42) [29].

$$\Gamma_a^t = \frac{\sqrt{\begin{matrix}|S_{11}+S_{12}e^{j\theta_2}+S_{13}e^{j\theta_3}+S_{14}e^{j\theta_4}+S_{15}e^{j\theta_5}+S_{16}e^{j\theta_6}+S_{17}e^{j\theta_7}+S_{18}e^{j\theta_8}|^2+\\ |S_{21}+S_{22}e^{j\theta_2}+S_{23}e^{j\theta_3}+S_{24}e^{j\theta_4}+S_{25}e^{j\theta_5}+S_{26}e^{j\theta_6}+S_{27}e^{j\theta_7}+S_{28}e^{j\theta_8}|^2+\\ |S_{31}+S_{32}e^{j\theta_2}+S_{33}e^{j\theta_3}+S_{34}e^{j\theta_4}+S_{35}e^{j\theta_5}+S_{36}e^{j\theta_6}+S_{37}e^{j\theta_7}+S_{38}e^{j\theta_8}|^2+\\ |S_{41}+S_{42}e^{j\theta_2}+S_{43}e^{j\theta_3}+S_{44}e^{j\theta_4}+S_{45}e^{j\theta_5}+S_{46}e^{j\theta_6}+S_{47}e^{j\theta_7}+S_{48}e^{j\theta_8}|^2+\\ |S_{51}+S_{52}e^{j\theta_2}+S_{53}e^{j\theta_3}+S_{54}e^{j\theta_4}+S_{55}e^{j\theta_5}+S_{56}e^{j\theta_6}+S_{57}e^{j\theta_7}+S_{58}e^{j\theta_8}|^2+\\ |S_{61}+S_{62}e^{j\theta_2}+S_{63}e^{j\theta_3}+S_{64}e^{j\theta_4}+S_{65}e^{j\theta_5}+S_{66}e^{j\theta_6}+S_{67}e^{j\theta_7}+S_{68}e^{j\theta_8}|^2+\\ |S_{71}+S_{72}e^{j\theta_2}+S_{73}e^{j\theta_3}+S_{74}e^{j\theta_4}+S_{75}e^{j\theta_5}+S_{76}e^{j\theta_6}+S_{77}e^{j\theta_7}+S_{78}e^{j\theta_8}|^2+\\ |S_{81}+S_{82}e^{j\theta_2}+S_{83}e^{j\theta_3}+S_{84}e^{j\theta_4}+S_{85}e^{j\theta_5}+S_{86}e^{j\theta_6}+S_{87}e^{j\theta_7}+S_{88}e^{j\theta_8}|^2\end{matrix}}}{2\sqrt{2}} \quad (1.43)$$

The phase excitations of port-2, 3, 4, 5, 6, 7, and 8 are varied from 0° to 360°. Let's consider an example for seven cases from Case-1 to Case-7 below.

Case-1: P^1=0°, P^2=0°, P^3=30°, P^4=60°, P^5=90°, P^6=120°, P^7=150°, P^8=180°
Case-2: P^1=0°, P^2=30°, P^3=60°, P^4=90°, P^5=120°, P^6=150°, P^7=180°, P^8=210°
Case-3: P^1=0°, P^2=60°, P^3=90°, P^4=120°, P^5=150°, P^6=180°, P^7=210°, P^8=240°
Case-4: P^1=0°, P^2=90°, P^3=120°, P^4=150°, P^5=180°, P^6=210°, P^7=240°, P^8=270°
Case-5: P^1=0°, P^2=120°, P^3=150°, P^4=180°, P^5=210°, P^6=240°, P^7=270°, P^8=300°
Case-6: P^1=0°, P^2=150°, P^3=180°, P^4=210°, P^5=240°, P^6=270°, P^7=300°, P^8=330°
Case-7: P^1=0°, P^2=180°, P^3=210°, P^4=240°, P^5=270°, P^6=300°, P^7=330°, P^8=360°

Finally, it evaluates the values of TARC corresponding to varying phase excitation and what will be the changes that occurred that show the effectiveness of the MIMO antenna.

1.7.2.6 Channel Capacity Loss (CCL)

In a MIMO system, the numbers of antenna elements are increased due to that high data rate, and maximum attainable channel capacity can be obtained, but the uncorrelated Rayleigh fading will be induced in MIMO channels, resulting in the loss of channel capacity. The CCL is estimated by using Eq. (1.44) [30].

$$C_{loss} = -\log_2 \det(\psi^R) \quad (1.44)$$

where $\Psi^R = [\rho_{ij}]$ is correlation matrix for the receiving antenna, $\rho_{ii} = 1 - |\sum_{n=1}^{N} S_{in}^* S_{ni}|$ and $\rho_{ij} = -|\sum_{n=1}^{N} S_{in}^* S_{nj}|$ for $(i,j), (i \neq j) \in (1,2,3,4,5,6,7,8 \ldots . N)$.

The correlation matrix can be elaborated in Eq. (1.45) for an example of 8×8 MIMO antenna, that is,

$$\psi^R = \begin{bmatrix} \rho_{11} & \rho_{12} & \rho_{13} & \rho_{14} & \rho_{15} & \rho_{16} & \rho_{17} & \rho_{18} \\ \rho_{21} & \rho_{22} & \rho_{23} & \rho_{24} & \rho_{25} & \rho_{26} & \rho_{27} & \rho_{28} \\ \rho_{31} & \rho_{32} & \rho_{33} & \rho_{34} & \rho_{35} & \rho_{36} & \rho_{37} & \rho_{38} \\ \rho_{41} & \rho_{42} & \rho_{43} & \rho_{44} & \rho_{45} & \rho_{46} & \rho_{47} & \rho_{48} \\ \rho_{51} & \rho_{52} & \rho_{53} & \rho_{54} & \rho_{55} & \rho_{56} & \rho_{57} & \rho_{58} \\ \rho_{61} & \rho_{62} & \rho_{63} & \rho_{64} & \rho_{65} & \rho_{66} & \rho_{67} & \rho_{68} \\ \rho_{71} & \rho_{72} & \rho_{72} & \rho_{73} & \rho_{74} & \rho_{75} & \rho_{76} & \rho_{78} \\ \rho_{81} & \rho_{82} & \rho_{83} & \rho_{84} & \rho_{85} & \rho_{86} & \rho_{87} & \rho_{88} \end{bmatrix}. \quad (1.45)$$

However, the above-discussed performance metrics are essential to evaluate the effectiveness of the MIMO antenna performances, where different antenna diversity dimensions are utilized in configuration of a MIMO antenna to enhance the signal quality.

1.8 MIMO Antenna Diversity Dimensions

In MIMO channel links, different signal data streams transmitted by multiple antennas takes multiple paths to arrive on another channel end of the multiple antenna's outputs. The signal data streams in the multipath environment correlated constructively and destructively by experiencing different phenomena like reflection, refraction, diffraction, interference, and scattering due to the presence of various obstacles lying on the transmission route. As a result, the effective received data streams as all would not get fading dip at the same time, degrades channel's performances. For the better reception of signal data streams in the multipath propagation environment, the antenna diversity principle is used at receiving end as follows [31].

The principle of antenna diversity is that multiple antenna outputs experience different data streams due to different channel conditions, and these data streams are only partially correlated. Thus, it is highly suitable that if one antenna is in the deep fade, the other is not and provides a sufficient signal [32]. As encountered with a blocked or shadowed direct line-of-sight (LOS) path in multipath propagation environment, where

each receive antenna experiences a different fading environment. Thus, multiple diversity dimensions can be deployed in the MIMO antenna utilized at the receiver terminal to improve the quality and reliability of the signals. These are mainly spatial diversity, polarization diversity, and pattern/angle diversity, as demonstrated in Fig. 1.10.

These diversity techniques provide two significant benefits: first, increased reliability in multipath channels, as fading in received signal experiences due to interference by reflected signals. The fade level observed on average for a given outage probability (percent downtime) is reduced through the diversity technique. The second is that it improves the average received signal power. Polarization or angle diversity automatically adjusts the antenna characteristics for maximum received signal due to improved efficiency of the radio link. However, the interference induced between the antenna element's signals in the above discussed different antenna diversity mainly due to the electromagnetic correlation between them and the source of electromagnetic coupling is expanded in the next section.

1.9 Electromagnetic Coupling in MIMO Antenna

The electromagnetic interference introduced between the antenna elements of the MIMO antenna defines electromagnetic mutual coupling when multiple patches are placed close to each other on a substrate having a unique metallic surface, i.e., planar or non-planar antennas, they are mutually coupled in different ways depending on the type of antennas and their arrangement.

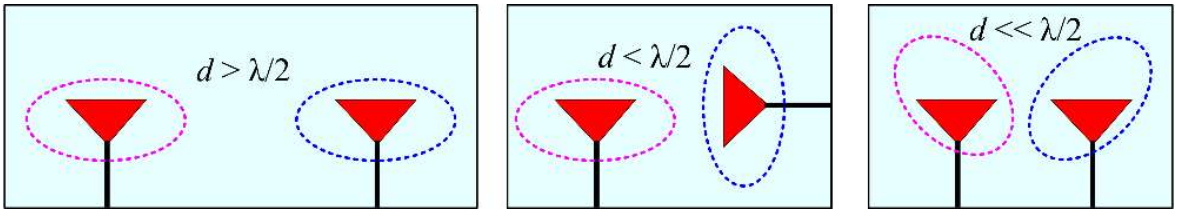

(a) (b) (c)

Fig. 1.10: MIMO antenna diversity dimensions (a) spatial diversity, (b) polarization diversity, and (c) pattern/angle diversity.

1.9.1 Electromagnetic Coupling Sources

Let's consider two coaxial fed antennas placed in four different arrangement scenarios for different possible mutual coupling sources between two radiators of any type, as demonstrated in Fig. 1.11. The primary sources of EMC in these arrangements are space waves, the surface waves propagating along with the dielectric/air interface, and the conducting current due to the presence of a metallic ground plane. If the structure is truncated, then surface waves and conducting currents are transformed into scattered waves as another type of EMC source, as all identified in [33]. When the antenna radiators are closely placed on a common substrate having a shared ground plane, strong electromagnetic coupling between them is observed, causing the high port to port coupling due to space wave, surface wave, and conducting wave, as shown in Fig. 1.11(a). As all the same as previous, only changes in the ground plane that keep partial shown in Fig. 1.11(b), eliminates the conducting wave effect that is an important source of coupling, still scattered wave from the edges of the partial ground cause of undesirable coupling. In Fig. 1.11(c), the antenna radiators are placed on the partial substrate having a common ground plane. As a result, coupling slightly reduces due to surface waves having no longer without any effect. Still, scattered waves from the edges of the substrate cause undesirable coupling. Finally, two different patch antennas are separated by a certain distance, as demonstrated in Fig. 1.11(d). In this configuration, surface waves and conducting waves totally absent as causing the lowest electromagnetic coupling are observed. However, the most significant sources of electromagnetic coupling are space waves and surface waves, while the effect of scattered waves and conducting waves have on longer. The presence of mutual coupling essentially depends on the placement of radiators, the separation between two antenna radiators ('d'), substrate parameters like thickness ('h'), and dielectric constant ('ε').

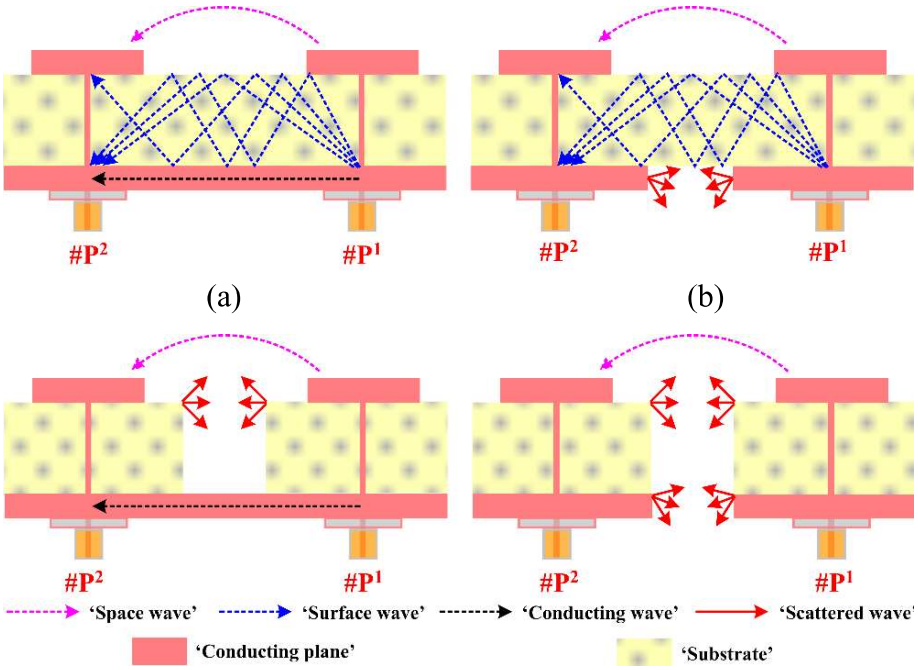

Fig. 1.11: Electromagnetic coupling between two coaxial-fed patch antennas (a) patches on the same substrate with common ground, (b) patches on a unique substrate with partial ground, (c) patches on a partial substrate with common ground, and (d) individual antennas.

1.9.2 Space Wave and Surface Wave Coupling

The mutual coupling between antenna elements is mainly derived from surface wave propagation. According to the electromagnetic (EM) wave propagation theory, the corresponding y-component of the electric field related to the surface wave traveling toward the + y direction that can be expressed as [34].

$$E(y,t) = E_0 e^{jyk}.e^{j\omega t} \tag{1.46}$$

$$k = \omega.\sqrt{\mu\varepsilon} \tag{1.47}$$

where, $e^{j\omega t}$ considering the time convention and E_0 is the amplitude of the surface wave, k is wavenumber in media, ω is the angular frequency of the traveling wave, μ and ε are effective permeability and effective permittivity related to media, respectively. The value of both (permeability and permittivity) is positive in the natural electromagnetic media, so the value of wavenumber will be a real number because electromagnetic waves can generally travel.

It is a well-established phenomenon that the use of a thicker substrate is responsible for enhancing the impedance bandwidth of the microstrip antenna. That is also responsible for generating the surface wave in the substrate might degrade the antenna's conventional performances. Let's assume, two closely spaced patch antennas sharing a common substrate having a separation between them *d*, there will be two types of coupling existing in the two-element antenna system [1]: first is the surface-wave coupling S_{21}^{sur} restricted inside the substrate, and second is the space-wave coupling S_{21}^{spa} restricted outside the substrate (above the patches). Hence, the total coupling S_{21}^{tot} is the combination of both, that is,

$$S_{21}^{tot} = S_{21}^{sur} + S_{21}^{spa} \tag{1.48}$$

where, all parameters defined in Eq. (1.48) have complex values. When S_{21}^{sur} and S_{21}^{spa} are in the same phase, they add together, giving a maximum S_{21}^{tot}. Conversely, when both are out of phase, they subtract together, providing a minimum S_{21}^{tot}.

The ratio of the magnitude of maximum radiated electric field on each patch in the two-element antenna system defines the space-wave coupling S_{21}^{spa}, as mention in [35].

$$S_{21}^{spa} = \frac{max(E_{spa})\ on\ secondary\ patch}{max(E_{spa})\ on\ primary\ patch} \tag{1.49}$$

where, E_{spa} is maximum radiated electric field for the case of most interest.

The significant contribution of space-wave coupling S_{21}^{spa} can be effectively controlled by managing separation distance between both radiator '*d*' and space permittivity 'ε_2.'

The effective surface waves coupling is mainly bound onto the interface defined by power ratio. As the power inside the substrate over the total power is expressed as power ratio '*P*' given by [36] that is,

$$P = \frac{\varepsilon_r k_y^3 [2k_{z1}h + sin(2k_{z1}h)]}{[\varepsilon_r k_y^3 \{2k_{z1}h + sin(2k_{z1}h)\} + k_{z1}^3 sin^2(k_{z1}h)]} \tag{1.50}$$

where h is the substrate thickness, and k_{z1} and k_y are the phase constants along the z- and y-directions, respectively.

Eq. (1.50) indicates that 'P' increases with the increase of 'h'. For thicker substrate $h = 0.25\lambda/\sqrt{\varepsilon_r}$, '$P$' will be around 0.6 means inside the substrate, 60% surface wave power is concentrated, leading to huge surface wave coupling. Under this scenario, the total coupling S_{21}^{tot} no longer decays with separation distance 'd' as a monotonic exponential curve. Besides, for thinner substrate $h < 0.1\lambda/\sqrt{\varepsilon_r}$, '$P$' will be less than 0.1 means inside the substrate, few portions of surface wave power is restricted as might be a weak surface wave coupling [37]. The influence of surface waves can be neglected by controlling 'P', which is satisfied by the given criterion for 'h.'

However, the above-discussed electromagnetic coupling sources induced in the MIMO configuration can be neutralized by utilizing the various developed mutual coupling reduction techniques.

1.10 Mutual Coupling Reduction Techniques

With the growth of the Internet of Things (IoT), user's devices have been becoming extremely compact/low-profile/slimmer, and multiple new features are growing due to the need for multiple antennas increasing in the receiver of the user devices. The space available to embed multiple antennas in the device is minimal because that antenna element is closely spaced. Therefore, an issue of electromagnetic mutual coupling between multiple antennas is induced. So, the reduction of mutual coupling between antenna elements is necessary and is more challenging for the research community. However, the mutual coupling reduction techniques have their own advantage and limitations. Apart from this, some 3-D methods are available in the literature that is not suitable for compact portable devices, increasing the complexity in terms of fabrication, implementation in the device's terminal, and mode of operation. Therefore, a simple

decoupling technique is needed, which is more reliable with the device's terminals in the different mode of operation.

Many mutual coupling reduction/isolation enhancement techniques are available in the literature, which are discussed in the state-of-the-art review section.

1.11 State-of-the-Art Review on MIMO Antenna

A brief literature review on the MIMO antenna based on printed planar monopole antenna elements is carried out. Which are related to the scope of the thesis and categorized in three-part such as 2-element, 4-element, and 8-element MIMO antenna as follows:

1.11.1 Review on Two-Element MIMO Antenna

In year 2002, two orthogonal diversity monopole radiators symmetrically placed on the T-shaped shared ground plane having a total antenna cross-section area of 100×50 mm^2 was presented for WLAN (2.4 GHz) band with mutual coupling between antenna elements is less than -31 dB [38]. Further, truncated square monopole radiator based two-element diversity MIMO antenna was proposed for WLAN application (2.4-2.484 GHz) with mutual coupling between antenna elements is less than -31 dB [39].

Thereafter in 2005, C-shaped monopole radiators was utilized to configure two-element diversity MIMO antenna having total cross-section area of 96×50 mm^2, applicable for the dual frequency band of WLAN (2.4/5.2 GHz), and it provides isolation between antenna elements is better than 25 dB in the dual frequency band [40].

In 2006, two-element MIMO antenna for the dual frequency band of WLAN (2.4/5.2 GHz) was reported, which consist of two double T-shaped monopole radiators placed on the top of the substrate and slit loaded rectangular common ground plane on the rear side of the substrate [41]. The isolation better than 15 dB was achieved between antenna elements. Dual band two-element MIMO antenna consist of two identical multi-

branch monopole radiators was presented [42]. T-shaped and dual inverted-L-shaped stub connected shared ground plane was used to enhance the isolation between antenna elements which was better than 13 dB and 16 dB respectively in the UMTS (1.92-2.17 GHz) and WLAN (2.4-2.484 GHz) band.

Two mirror-identical elliptical monopole radiators were proposed to configure two-element MIMO antenna for wideband (2.3-5.9 GHz). Dual arrow-shaped ground stubs (below the radiators) were connected to the slit-loaded ground plane for suppressing the mutual coupling between them. The obtained mutual coupling is less than -17dB in the respective band [43]. Similarly, two mirror-identically right-tringle monopole radiators were proposed for UWB (3.1-10.6 GHz) application having a total cross-section area of 35×40 mm^2 [44], A tree-shaped ground stub between the radiators is used for low mutual coupling which was better than -16 dB.

Thereafter, two-element UWB-MIMO antenna consists of two orthogonal rectangular monopole radiators having split-ring shaped slot-loaded ground were proposed. It provides the minimum isolation value of 15 dB [45].

In 2011, circular monopoles radiator-based two-element MIMO antenna was proposed for UWB applications. An inverted Y-shaped ground stub was connected at the centre of the common ground to reduce the mutual coupling between them, which is better than -15 dB [46]. Further in the same year, two identically mirrored meander monopole radiators were proposed to configure a two-element MIMO antenna [47]. Two I-shaped ground stubs were connected with the discrete rectangular ground plane between the radiators for low mutual coupling. Which provides S_{11} < -10 dB and S_{21} < -12 dB for 760-886 MHz band.

Thereafter in 2012, two symmetrically mirrored monopole radiators based compact two-element MIMO antenna for wideband (2.4-6.55 GHz) were presented. Dual bent slits

loaded I-shaped stub connected ground plane were used for reducing the coupling between antenna elements, which is better than -18 dB [48]. Followed by, 4-shaped monopole radiators based two-element MIMO antenna for dual long-term evolution (LTE) band of 803–823 MHz and 2440–2900 MHz were proposed in 2012 [49]. Spiral loaded defected ground structure (DGS) was used to reduce the coupling between antenna elements, which is better than -17 dB and -9 dB in the lower and higher frequency band, respectively. Afterwards, a pair of symmetrically mirrored crooked monopole radiators were used to configure a compact two-element MIMO antenna for 2.4 GHz band application [50]. T-shaped neutralized stub was connected with monopole radiators to reduce the coupling between them, which is better than -28.9 dB. Followed by, orthogonally placed two identical square monopole radiators were presented for UWB (3.1-10.6 GHz) [51]. Dual inverted L-shaped and I-shaped ground stub were connected with a shared ground plane for reducing the coupling between a pair of elements, which is better than -15 dB.

In 2014, a pair of symmetrically mirrored half-circle-based quasi-self-complementary antennas (QSCA) was demonstrated for UWB application [52]. Dual slit-loaded inverted T-shaped ground stub connected ground plane was utilized for mutual coupling reduction between antenna elements, which is better than -15 dB. Further, orthogonally placed a pair of identical dual slits loaded rectangular monopole radiators was illustrated for UWB (3.1-10.6 GHz) [53]. Dual inverted L-shaped and I-shaped slits were created in the ground to reduce the coupling between a pair of elements, which is better than -15 dB.

In 2015, a pair of identical T-shaped radiators placed orthogonally on a square slot-loaded square ground plane was demonstrated for UWB (3.1-10.6 GHz) application [54]. A parasitic T-shaped stub was placed between antenna elements to reduce the coupling

between them, which is better than -15 dB. Further, two identical (a combination of half circular ring and half square ring) monopole antenna with inverted L-shaped stub connected partial ground were placed on substrate cross-section area of 24×42 mm^2 in four different cases to form a two-element UWB MIMO antenna for automotive communication [55]. In all considered cases, a minimum isolation value of 15 dB was obtained between antenna elements in the respective band.

In 2016, two identical circular monopole radiators based two-element wideband MIMO antenna were proposed for 3.1-5.0 GHz band [56]. A neutralization network was used to reduce the mutual coupling between antenna elements, which is better than -22 dB. Followed by, DGS-based dual notched-band polarization diversity two-element MIMO slot antenna for UWB application was proposed [57]. A Y-shaped slit is etched on the ground plane between orthogonal feed lines, which provides improved impedance matching and low mutual coupling (better than -15 dB) in the 3.5-10.6 GHz band. The polarization diversity was achieved by using orthogonal feed line.

In 2017, two identical circular monopole radiators based on a two-element MIMO antenna were proposed. A carbon black film was coated to reduce the mutual coupling between antenna elements. It has S_{11} < -10 dB for 2.5-11 GHz and S_{21} < -15 dB [58]. Thereafter, Khan *et al.* [59] presented the two-element MIMO antenna with a cross-section area of 23×29 mm^2 consists of a pair of symmetrically mirrored triangular monopole radiators placed at the top of the substrate and inverted L-shaped ground stubs connected to shared ground was created at the bottom of the substrate. To reduce the coupling complementary split-ring resonator (CSRR) was utilized on the ground between the antenna elements. It provides $S_{ij} \in i=j$ < -10 dB for 3-12 GHz and $S_{ij} \in i \neq j$ < -15 dB.

Two identical mirrored radiators based UWB MIMO antenna were reported. Dual F-shaped ground stubs was introduced in the shared ground plane between antenna

elements to reduce the mutual coupling between them. It gives $S_{ij} \in i \neq j < -20$ dB in the respective band [60]. Thummaluru *et al.* [61] investigated two identical mirrored F-shaped MIMO antenna having a total cross-section area of 48×48 mm^2. The ground plane of the conventional monopole antenna was replaced by frequency selective surface (FSS) to reduce the coupling and radar cross-section (RCS) simultaneously. Further, Chandel *et al.* [62] presented a compact two-element MIMO antenna for super ultrawideband with a total cross-section area of 18×34 mm^2 consisting of a pair of symmetrically mirrored monopole radiators and inverted L-shaped ground stubs connected to the shared ground plane. It has $S_{ij} \in i=j < -10$ dB of 2.9-20 GHz and $S_{ij} \in i \neq j < -22$ dB.

Two symmetrical microstrips line-based two-element Vivaldi MIMO antenna were proposed for UWB application [63]. A T-shaped ground slit was introduced in the shared ground plane between the feed line to reduce the mutual coupling between them. It has $S_{ij} \in i=j < -10$ dB of 2.9-11.6 GHz and $S_{ij} \in i \neq j < -16$ dB. Ghannad *et al.* [64] studied two identical closely spaced rectangular microstrip antenna-based two-element MIMO antenna having a total cross-section area of 22×33 mm^2. The isolation and impedance matching were simultaneously improved by connecting two T-shaped stubs to the feeds line and a rectangular stub between them. Wang *et al.* [65] presented two half-cutting slit loaded circulars 180^0 mirrored MIMO antenna for UWB having the cross-section area of 35×50 mm^2. A fence-type structure was introduced in the shared ground between antenna elements to reduce the mutual coupling. It has $S_{ij} \in i=j < -10$ dB of 3-11 GHz and $S_{ij} \in i \neq j < -25$ dB.

The review literature of the two-element MIMO antennas based on monopole element is studied. Chapter 2 of the thesis origination is based on that literature study.

1.11.2 Review on Four-Element MIMO Antenna

Karimian *et al.* [66] presented four-element MIMO antenna consisting of novel L-shaped slot dipole and L-shaped slit for WLAN (2.4 GHz and 5.2 GHz) and WiMAX (3.5 GHz). The WLAN band was achieved by L-shaped slot whereas 3.5 GHz was achieved by the introduction of L-shaped slits. A high isolation value of 16 dB between MIMO elements was achieved by orthogonal placement for closely spaced antenna elements ($< 0.05\lambda$).

Thereafter, a compact four-element MIMO antenna was proposed for WiMAX application [67], consisting of four symmetrically L-shaped monopole antenna elements orthogonally placed on the discrete ground plane. The isolation between antenna elements was improved by using split-ring resonator. Followed by, a four-element MIMO antenna with common elements was proposed with a total cross-section area of 120×140 mm^2 for Wi-Fi, WiMAX, and LTE application, which consisting of four orthogonal microstrip feed line printed monopole antennas with common radiating element and a ring-shaped ground plane [68]. The ground plane is modified by introducing four slots in each corner of the antenna to reduce the mutual coupling between antenna elements. The reflection bandwidth (-10 dB) was observed to be 1100 MHz, i.e., 1.8-2.9 GHz. The measured isolation was achieved better than 15 dB using a modified ground plane.

In year 2015, Koch fractal monopole antennas with I-shaped stub connected discrete ground plane was placed on a substrate cross-section area of 45×45 mm^2, forming four-element UWB MIMO antenna [69] and orthogonally placement of antenna elements provided low coupling between antenna elements. The impedance bandwidth (S_{11} < -10 dB) was obtained from 2 GHz to 10.6 GHz with isolation better than 17 dB over the entire UWB.

Thereafter, a pair of symmetrically same oriented monopole antenna elements with dual stepped-shaped slit loaded ground plane was unitized to configure a four-element

MIMO antenna for UWB application [70], which consists of the dual two-element antenna placed 180^0 mirrored (out face orientation) with common ground plane on a substrate cross-section area of 42×25 mm^2. The measured impedance bandwidth (S_{11} < -10 dB) of UWB was achieved from 3.1 GHz to 12 GHz with isolation value better than 22 dB over the entire UWB. Followed by, Anitha *et al.* [71] presented a monopole antenna element with the slotted ground plane was orthogonally rotated on a substrate cross-section area of 45×45 mm^2, forming a four-element MIMO antenna with the discrete ground plane. A split-ring resonator (SRR) with antenna elements was used to reduce the mutual coupling between antenna elements. The MIMO antenna achived impedance bandwidth (S_{11} < -10 dB) from 2.2 GHz to 6.28 GHz with mutual coupling better than -14 dB in the respective band.

Further, four inverted L-monopole antenna elements with rectangular ground were orthogonally placed on a substrate cross-section area of 40×40 mm^2, forming four-element MIMO antenna and discrete ground plane of them connected through a copper strip to make share ground plane. The MIMO antenna achived impedance bandwidth (S_{11} < -10 dB) from 2.7 GHz to 4.94 GHz with isolation value better than 11 dB (without any decoupling structure) in the respective band [72]. Similarly, in [73] four inverted L-monopole antenna elements with rectangular ground were orthogonally placed on a substrate cross-section area of 40×40 mm^2, forming four-element dual-band MIMO antenna and discrete grounds of them connected through a copper strip to make share ground plane. A split-ring resonator (SRR) was utilized with inverted-L monopole to reduce the mutual coupling between antenna elements, resulting in better than 14 dB isolation obtained in the respective dual-band.

Four rectangular microstrip antenna elements were orthogonally placed on a substrate cross-section area of 32×32 mm^2, forming a four-element dual-band MIMO

antenna with a shared ground plane. A plus-shaped metalized vias and the metalized wall between antenna elements were introduced to reduce the mutual coupling between them. The measured resonant frequency is centred at 3.5 and 5.7 GHz with bandwidth of 58 MHz and 43 MHz, respectively with measured isolation value of 18.4 dB and 22.7 dB in the respective bands [74]. Further, four symmetrical elements orthogonally placed on a substrate cross-section area of 50×50 mm^2 having a slot-loaded common ground plane, forming four-element MIMO antenna for 5G sub-6 GHz application [75]. It has $S_{ij} \in i=j <$ -10 dB for 3.4-3.8 GHz and $S_{ij} \in i \neq j <$ -12 dB in the respective band. Similarly, four symmetrical elements orthogonally placed on a substrate cross-section area of 26×26 mm^2 having a slot-loaded common ground plane, forming a compact four-element MIMO antenna for WLAN application [76]. The MIMO antenna operated ($S_{11} <$ -10 dB) at 5.6-5.8 GHz with isolation better than 15.4 dB.

Saad and Mohamed [77] proposed the four-element asymmetrically placed four-element slot antenna array. The presented MIMO exhibited impedance bandwidth ($S_{11} <$ -10 dB) for 2.94-14 GHz with port to port isolation between them 17 dB over the entire band. This was achived without any decoupling structures. After that, Alam *et al.* [78] proposed a design of 5G sub-6 GHz (2.5-4.2 GHz) application-based four-element MIMO antenna for cognitive radio with three selected modes, consisting of four symmetrical monopole antenna elements orthogonally placed having the discrete ground plane. Further, four semi-elliptical monopole antenna elements orthogonally placed on a uniplanar substrate cross-section area of 38.3×38.3 mm^2, forming four-element UWB MIMO antenna with inverted L-shaped ground planes [79]. A set of slits was created in the ground to reduce the correlation between antenna elements. The MIMO antenna achieved $S_{ij} \in i=j <$ -10 dB of 3-13.2 GHz and $S_{ij} \in i \neq j <$ -17 dB in the respective band.

In 2020, four modified monopole elements orthogonally placed on a substrate cross-section of 40×40 mm^2, having four discrete inverted L-shaped stubs connected grounds was utilized to configure four-element circularly polarized MIMO antenna for wearable biotelemetric devices (2.40-2.48 GHz) [80]. The antenna exhibited 3 dB CP bandwidth of 1300 MHz and 1040 MHz in free space and body worn, respectively. It has $S_{ij} \in i \neq j$ < -26 dB in the respective band. Later, a 5G sub-6 GHz application-based four-element circularly polarized MIMO antenna was proposed with a total cross-section area of 60×60 mm^2 [81]. Each element consists of a 50 Ω microstrip feed line element placed on the top and at the bottom of the substrate, a slit-loaded ground plane integrated with two rectangular arms for realizing circular polarization. A pair of symmetrically same oriented monopole antenna elements 180^0 mirrored (out face orientation) and discrete ground of them connected through inverted H-shaped strip. It secured $S_{ij} \in i=j$ < -10 dB of 3.4-3.8 GHz and $S_{ij} \in i \neq j$ < -19 dB. Further, an optically transparent four-element MIMO antenna for 5G mm-wave application was proposed on a substrate cross-section area of 24×20 mm^2 [82]. A pair of symmetrically same oriented slot-loaded microstrip antenna elements 180^0 mirrored (out face orientation) with a shared ground plane. It secured $S_{ij} \in i=j$ < -10 dB of 24.1-27.18 GHz and 33-44.13 GHz, and $S_{ij} \in i \neq j$ < -16 dB in the respective dual-band.

The literature review on the four-element MIMO antennas is carried out. Based on that, Chapter 3 of the present thesis origination is presented.

1.11.3 Review on Eight-Element MIMO Antenna

A pair of circular-openings monopole radiators having the same orientation was orthogonally placed on a rectangular substrate cross-section area of 60×93 mm^2 with the discrete ground plane, forming an eight-element UWB MIMO antenna [83]. In this design, a closed-loop frequency selective surface (CL-FSS) and quad strip-connected

circular arc are used as decoupling structures in the ground plane to reduce the coupling between antenna elements. The eight-element MIMO antenna achieved reflection coefficient/impedance bandwidth $S_{ij} \in i=j$ < -10 dB of 3.1-10.6 GHz and the mutual coupling better than -15 dB in the respective band.

Thereafter, a pair of mirrored inverted-F antenna was orthogonally placed on a square substrate cross-section area of 33×33 mm^2 having a uniplanar ground plane, forming an eight-element MIMO antenna based on inverted-F antenna for WLAN application [84]. A set of slit and capacitor pairs was used to generate additional LC resonance, which decreases the mutual coupling between the antenna elements. The impedance bandwidth S_{11} < -10 dB is observed from 4.86-5.27 GHz and isolation better than 30 dB in the respective band. Later, two symmetrical sets of a four-element MIMO antenna were placed on a rectangular substrate cross-section area of 38×90 mm^2 having the discrete ground plane, forming an eight-element MIMO antenna for UWB application [85]. A four-element MIMO antenna consists of modified circular monopole antenna elements with I-shaped stub connected discrete ground plane were orthogonally placed on a substrate cross-section area of 38×38 mm^2. A single element consists of an annular ring and circular disc shorted to the ground by metalized via holes. The eight-element MIMO antenna achieved $S_{ij} \in i=j$ < -10 dB of 3-15 GHz and $S_{ij} \in i \neq j$ < -16 dB in respective band.

In 2018, two symmetrical sets of four inverted-L and top-hat-shaped monopole antennas were placed on two sides of the common ground plane, forming an eight-element 5G sub-6 GHz MIMO antenna with an overall size of 38×90 mm^2 [86]. Pattern diversity is used to reduce the coupling between antenna elements. The eight-element MIMO antenna secured $S_{ij} \in i=j$ < -10 dB of 3.5-3.6 GHz and $S_{ij} \in i \neq j$ < -15 dB in the respective band.

Further, a set of two identical mirrored modified rectangular open-loop resonating radiators with open slot-loaded common ground was orthogonally placed on a square substrate cross-section area of 38×90 mm^2, forming eight-element circularly polarized MIMO antenna with slit-loaded shared ground plane [87]. The eight-element MIMO antenna secured $S_{ij} \in i=j$ < -10 dB of 5.08-5.95 GHz and $S_{ij} \in i \neq j$ < -20 dB in the respective band. Later, two symmetrical sets of a four-element MIMO antenna were placed on a rectangular substrate cross-section area of 58×128 mm^2 having the discrete ground plane with 12 mm separation between both sets, forming eight-element MIMO antenna for super wideband (SWB) application [88]. A four-element MIMO antenna consists of spade-shaped monopole antenna elements with discrete ground plane were orthogonally placed on a substrate cross-section area of 58×58 mm^2. A windmill-shaped decoupling structure is used between antenna elements to reduce mutual coupling between antenna elements. The eight-element MIMO antenna achieved $S_{ij} \in i=j$ < -10 dB of 2.9-40 GHz and $S_{ij} \in i \neq j$ < -17 dB in the respective band.

The literature review on the planar structure-based eight-element MIMO antennas is studied. Based on that, Chapter 4 of the thesis origination is proposed.

1.11.4 Review on Integrating Different Antennas on a Common Aperture

In year 2019, integrating of a two-element MIMO antenna and a 1×4 slot array antenna on a common-aperture cross-section area of 70×50 mm^2 were proposed for triple frequency band operation [89]. A two-element MIMO antenna consists of two identical mirrored monopole radiators with shared ground placed in the same orientation on a common aperture. It secured dual $S_{ij} \in i=j$ < -10 dB of 2.45-2.85 GHz (4G) and 3.18-3.68 GHz (5G). A tapered slot array antenna (1×4-array) was introduced between MIMO elements on the same aperture for 5G mm-wave. It secured $S_{ij} \in i=j$ < -10 dB of 25-30 GHz. The open-ended tapered slot is created in the partially shared ground plane to

reduce the coupling between antenna elements, which is observed better than -25 dB in the respective triple band. Further in the same year, integration of a dipole antenna and tapered slot antenna on a common-aperture cross-section area of 75×25 mm^2 were proposed for dual frequency band operation of 5G sub-6 GHz (at 3.6 GHz) and mm-wave (at 28 GHz) [90]. A dipole antenna is fed by a modified balun consisting of a tapered slot and microstrip line. The tapered slot provides the dual operation that first excites the dipole antenna at 3.6 GHz, and the second act as a slot antenna at 28 GHz.

Two different sets of four-element MIMO antenna were integrated on the same substrate cross-section area of 60×60 mm^2 formed an eight-element MIMO antenna for two different bands [91]. A set of four-element MIMO antenna consists of the complimentary-split-ring resonator (CSRR)-loaded inverted L-monopole antenna elements with L-shaped discrete ground plane were orthogonally placed at the corner on a substrate cross-section area of 60×60 mm^2, which is applicable for $S_{ij} \in i=j$ < -10 dB of 3.2-4.08 GHz and $S_{ij} \in i \neq j$ < -15 dB. Similarly, another set of four-element MIMO antenna consists of complimentary two L-shaped stub-loaded monopole feed elements with stepped-shaped discrete ground plane were orthogonally placed at the middle on the same substrate. It has $S_{ij} \in i=j$ < -10 dB of 3.2-5.32 GHz and $S_{ij} \in i \neq j$ < -15 dB. As per authors' knowledge limited papers are available in the literature for the integartion of 5G sub-6 GHz and mm-wave antennas.

In view of the above literature review, integration of two different MIMO antennas structures on a common aperture is proposed in Chapter 5 of the thesis.

1.12 Objective, Scope, and Structure of the Thesis

The objective of the thesis is first to understand what vital aspect to consider in designing a MIMO antenna and what performance metrics need to be enhanced. To this end, try to identify the aforementioned issues that occurred in the design and development of a

MIMO antenna and what mechanism to be used to rectify them. One of the main issues in designing a compact MIMO antenna is to achieve low mutual coupling/correlation between closely-spaced antenna elements. The coupling reduction techniques are studied, and responsible factors are identified. But some technique increases the implementing complexity in the device's terminals. Therefore, try to identify and develop a simple technique that is suitable and effective to reduce the coupling between antenna elements simultaneously reduce the implementation complexity as like pattern diversity, ground stubs, parasitic elements, slits, slots, etc.

In first step, identify a compact, low-profile, multi-standard antenna that is easily configured to multi-element, rotate in any direction, and integrate with portable user's terminals. The monopole antenna follows this criterion and is also suitable for omnidirectional coverage. In next step, design and development of a compact/low-profile MIMO antenna by utilizing a monopole antenna which should be most appropriate for modern scenario-based portable devices. Further, analysed the obtained performances (conventional and diversity) are following the standard criterion or not. Furthermore, increasing the number of antenna elements in the MIMO antenna configuration simultaneously improving operating impedance bandwidth will ensure a high capacity, data rate, and spectral efficiency following the capacity theorem.

In this process, design and development of the compact, low-profile MIMO antennas are simulated and experimentally validated. The simulation studies are performed using ANSYS HFSS (high frequency structure simulator) version 2020 R1. The prototype is fabricated by using the MITS-Eleven Lab printed circuit board (PCB) machine and *S*-parameters characteristics are measured by Anritsu's Vector Network Analyzer (model: *MS2038C*) and Keysight FieldFox Microwave Analyzer (model: *N9951A*).

The contributory thesis works as Chapters 2, 3, 4, and 5 present different application-based high-order MIMO antennas considering the main key objectives of the operating impedance bandwidth and the number of the antenna elements. These are continuously enhanced chapter-wise without compromising any aspect, which fulfils the goal of the thesis and ensures research scope for the future. With this introductory chapter, the remaining chapters of the thesis works are presented and organized in the following manner.

Chapter 2 presents a realization of 12-elements MIMO antenna for 5G smartphones, which is configured by utilizing a compact, low-profile two-element MIMO antenna. It provided satisfactory performances and will ensure high channel capacity and data rate.

Chapter 3 presents a 20-element MIMO antenna for localization system, which is configured by utilizing a compact, low-profile four-element wideband MIMO antenna. It obtained satisfactory performances and will ensure higher channel capacity and data rate than previous.

Chapter 4 presents a realization of 32-element MIMO antenna for internet of vehicle (IoV) application configured by utilizing a compact, low-profile eight-element ultra-wideband MIMO antenna and achieved satisfactory performances. It will ensure higher channel capacity and data rate than previously both.

Chapter 5 presents two different MIMO antenna integrated on a common aperture, further integrated inside the 5G smartphone's back cover which is configured by utilizing an extremely low-profile eight-element MIMO antenna (5G sub-6 GHz) and 1×4 array-based quad-element MIMO antenna (5G mm-wave) that will ensure high capacity and data rate by 5G-MIMO technique.

Finally, the investigations and concluding remarks carried out in the preceding chapter are summarized, emphasizing the scope for future research works in this domain presented in the last **Chapter 7.**

The structure of the thesis work is illustrated chapter wise in Fig. 1.12, i.e., Chapter 2 to Chapter 5.

Fig. 1.12: The structure of the present thesis works.